Dual thermal ecotypes detected within a nearly genetically-identical population of the unicellular marine cyanobacterium *Synechococcus*

Joshua D. Kling[1], Michael D. Lee[2,3], Eric A. Webb[1], Jordan T. Coelho[1], Paul Wilburn[2,4], Stephanie I. Anderson[5], Qianqian Zhou[6], Chunguang Wang[6], Megan D. Phan[1], Feixue Fu[1], Colin T. Kremer[4], Elena Litchman[4], Tatiana A. Rynearson[5], David A. Hutchins[1]

[1]*Department of Biological Sciences, University of Southern California, Los Angeles, CA 90007, USA*

[2]*Exobiology Branch, NASA Ames Research Center, Mountain View, CA 94035, USA*

[3]*Blue Marble Space Institute of Science, Seattle, WA 98154, USA*

[4]*Kellogg Biological Station, Michigan State University, Hickory Corners, MI 49060, USA*

[5]*Graduate School of Oceanography, The University of Rhode Island, Kingston, RI 02881, USA*

[6]*Third Institute of Oceanography, Ministry of Natural Resources, Xiamen, 361005, Fujian, China*

***Corresponding Author:**

David A. Hutchins

Address: 3616 Trousdale Parkway, AHF 207, Los Angeles, CA 90007

Email: dahutch@usc.edu

Keywords: *Synechococcus* | temperature adaptation | Intraspecific diversity | phycocyanin

Author Contributions:

Isolates were collected by JDK, PW, SIA, EL, TAR, & DAH, and subsequent culture work and its analysis done by JDK, MDP, EAW, FU, CTK. DNA extraction, sequencing, and analysis performed by JDK, MDL, JTC, QZ, & CW. All authors contributed to the writing.

24 **Significance**

25 Numerous studies exist comparing the responses of distinct taxonomic groups of marine
26 microbes to a warming ocean (interspecific thermal diversity). For example, *Synechococcus,* a
27 nearly globally distributed unicellular marine picocyanobacterium that makes significant
28 contributions to oceanic primary productivity, contains numerous taxonomically distinct lineages
29 with well documented temperature relationships. Little is known though about the diversity of
30 functional responses to temperature within a given population where genetic similarity is high
31 (intraspecific thermal diversity). This study suggests that understanding the extent of this
32 functional intraspecific microdiversity is an essential prerequisite to predicting the resilience of
33 biogeochemically essential microbial groups such as marine *Synechococcus* to a changing
34 climate.

35

Abstract

The extent and ecological significance of intraspecific diversity within marine microbial populations is still poorly understood, and it remains unclear if such strain-level microdiversity will affect fitness and persistence in a rapidly changing ocean environment. In this study, we cultured 11 sympatric strains of the ubiquitous marine picocyanobacterium *Synechococcus* isolated from a Narragansett Bay (Rhode Island, USA) phytoplankton community thermal selection experiment. Despite all 11 isolates being highly similar (with average nucleotide identities of >99.9%, with 98.6-100% of the genome aligning), thermal performance curves revealed selection at warm and cool temperatures had subdivided the initial population into thermotypes with pronounced differences in maximum growth temperatures. Within the fine-scale genetic diversity that did exist within this population, the two divergent thermal ecotypes differed at a locus containing genes for the phycobilisome antenna complex. Our study demonstrates that present-day marine microbial populations can contain microdiversity in the form of cryptic but environmentally-relevant thermotypes that may increase their resilience to future rising temperatures.

51 **Introduction**

52 Marine bacteria control most marine biogeochemical cycles (1, 2) and are composed of
53 an estimated 10^{10} species (3). In addition, bacterial species complexes also include numerous
54 strains or ecotypes (4–8). Much of the work documenting the ecological relevance of
55 intraspecific microdiversity has used amplified marker genes such as the 16S rRNA gene,
56 resolved to single base pair differences (9). However, there is still much work to be done to
57 describe the potentially substantial genotypic and (more importantly) phenotypic diversity that
58 exists within groups that are highly similar or even identical at the 16S rRNA level. At higher
59 taxonomic levels, microbial interspecific diversity has a recognized role increasing the stability
60 of biogeochemical cycling and resilience to a changing environment (10). In order to understand
61 the ability of microbial populations to persist and maintain their functional roles under changing
62 thermal regimes, however, it is also important to understand how much unrecognized
63 microdiversity relevant to future warmer temperatures currently exists within microbial
64 populations (11–13).

65 Efforts to understand the interactions of microbes with the marine environment have
66 often relied on approaches that underestimate or mask intraspecific diversity. For instance,
67 culture-based methods are often limited to a handful of strains that are amenable to cultivation or
68 are currently available in culture collections. These are then used to make generalizations about
69 the activity of a broader taxonomic group (14–16). Sequencing approaches avoid this culturing
70 bottleneck but lack the ability to provide rate measurements. Furthermore, metagenomic or
71 metatranscriptomic analysis pipelines often are unable to discern sequencing errors from rare
72 genotypes or strains (17). In addition, purely sequence-based *in situ* approaches are also limited
73 in the amount of ecotype microdiversity they can reveal, simply because detection relies on

74 observed correlations between relative abundance and ambient environmental parameters (e.g.
75 temperature, nutrients, light). Thus, rare ecotypes with optimal niches that lie outside of current
76 conditions will remain cryptic unless the environment changes. For example, most marine
77 microbial communities will undergo future selection by temperatures exceeding those that they
78 currently experience (18, 19), as current climate models predict that anthropogenic carbon
79 emissions will raise sea surface temperatures ~4°C by the year 2100 (20).

80 Marine unicellular picocyanobacteria are particularly important to our understanding of
81 how microbially mediated biogeochemical cycling will change with rising sea surface
82 temperatures (SST). The unicellular marine cyanobacterium *Synechococcus* is a major microbial
83 functional and taxonomic group that is found from the equator to high polar latitudes (8, 21).
84 This widespread and diverse genus is responsible for an estimated 16.7% of marine primary
85 production, and is expected to increase in both abundance and distribution as result of climate
86 warming (22). It has also been strongly correlated with carbon export to the deep ocean (23),
87 making this genus an important component of the marine carbon cycle.

88 In this study, we used multiple temperature incubations of a natural coastal assemblage to
89 enrich for 'thermal specialist' strains of *Synechococcus.* We then isolated multiple sympatric
90 strains from the contrasting temperature incubations and characterized their thermal niches,
91 allowing us to recover two co-occuring but distinct thermal phenotypes from a single initial
92 water sample. Finally, we used high-coverage, short read sequencing to obtain high-quality draft
93 genomes for all of the isolates. Upon comparing their assemblies, the two sets of thermally-
94 distinct isolates are nearly identical, with an average nucleotide identity (ANI) > 99.9%
95 demonstrating that these thermotypes belong to the same population. We additionally detected
96 genetic variation that differentiates both thermotypes in a locus coding for the photosynthetic

97 accessory pigment C-phycocyanin. This trait's relevance is not immediately apparent within the
98 current study's context, but is nevertheless strongly correlated with the identifiable thermal
99 specializations observed in this population.

100 **Results**

101 Out of the 11 strains of *Synechococcus* isolated in this study, one originated from our
102 initial cell sorting of the collected seawater (at 22°C), before nutrients were added (Table S1).
103 The other ten isolates were collected from the enrichment experiments, five from an 18 °C
104 enrichments and five from 30 °C. Because the 22°C *in situ* conditions and 18°C experimental
105 treatment represent temperatures that currently occur in Narragansett Bay, these isolates are
106 considered together and are referred to as "cool temperature isolates" and compared against
107 "warm temperature isolates" collected from 30 °C (a temperature exceeding those currently
108 recorded at this sampling site). Despite these considerable differences in temperature, all of the
109 cool and warm temperature isolates shared virtually identical morphologies (Table S1).
110 Picocyanobacteria were also detected in 22 and 26 °C temperature incubation treatments, but cell
111 sorting did not produce any culturable isolates from these incubations.

112 After growing each of the 11 isolates across multiple temperatures, we generated thermal
113 performance curves for each isolate, with an average R^2 of 0.81 (±0.14 SD, Figure 1A & S1;
114 Table S2). The average thermal maximum (Tmax) was highest for warm temperature isolates
115 (35.6 °C, ±0.5 SD) compared to cool temperature isolates (33.5 °C, ±0.9; t-test, $p = 0.005$; Figure
116 1B; Table 1). The optimal growth temperature (Topt) was also higher for isolates from warm
117 temperatures, with a mean of 29.8° (±1.8 SD), than for cool temperature (27.6 °C, ±1.2 SD);
118 however, this difference was not statistically significant ($p = 0.06$). Minimum growth
119 temperature (Tmin) and niche width (Tmax – Tmin) did not significantly differ between the two

120 groups ($p = 0.91$). In addition to differences in growth observed using *in vivo* fluorescence
121 measurements, we compared one warm and one cool temperature isolate (LA127 and LA31
122 respectively) when temperature was increased from 22 to 28 °C, closer to their Topt (Table S2).
123 This showed that the warm-temperature isolate accumulated ~2x more volume-normalized
124 particulate organic carbon (POC; $p = 0.002$; Figure S2A) and maintained a higher, but not
125 statistically significant ($p = 0.07$), growth rate (Figure S2B).

126 To compare genomic differences between cool and warm temperature isolates, sequence
127 data for each isolate collected from this study (n=11) was assembled and manually curated
128 producing estimated 100% complete draft genomes (Table S3). Recovered short read genomes
129 (hereafter called draft assemblies) were 2.74 Mbp long (±0.01 SD), split between an average of
130 22.1 (±6 SD) contigs with a mean GC content of 63.3% (±0.00) and mean gene count of 2976.0
131 (±11 SD) for each isolate. We generated long reads for one cool (LA31) and one warm
132 temperature isolate (LA127) and were able to close the genome of the warm temperature isolate
133 (one contig 2.75 Mbp long compared to 27 contigs from the short-read only assembly). Including
134 long reads substantially improved the assembly of the cool temperature isolate, reducing the
135 number of contigs from 18 to six (Table S3).

136 When constructing a phylogenetic tree with all presently available *Synechococcus*
137 genomes (Figure S2), the isolates from this study fell within the same clade as marine subcluster
138 5.2. With the level of resolution provided by 239 concatenated amino acid sequences, all 11 were
139 nearly indistinguishable from each other (Figure 2A). Interestingly, the most closely related
140 isolate in Genbank was CB0101 from Chesapeake Bay, another large coastal estuary located on
141 the east coast of the United States (24). High genetic relatedness was even more apparent using
142 average nucleotide identity (ANI), with greater than 99.99% (±0.003 SD) across 98.6-100% of

143 the assembly for all genomes (Figure 2B). For comparison, the average ANI between isolates
144 from this study and CB0101 was 85.46%.

145 Despite the high degree of similarity, when comparing draft assemblies from a
146 pangenomic perspective, 62 out of 2985 gene clusters were identified by Anvi'o (Figure S4,
147 Table S4) as having less than 100% functional (e.g. differences in sequence) or structural (e.g.
148 insertions, deletions) homogeneity between one or more assemblies. Manually examining these
149 gene clusters for genomic differences that correlated with isolation temperatures and measured
150 thermal performance curves revealed that many of the features causing this detected variation
151 were typically found only in one or a few isolates (Figure S5).

152 Only two gene clusters examined had patterns of variation that correlated with the
153 temperature treatments that these strains were isolated from (e.g. exclusive to warm temperature
154 isolates). These two gene clusters contain genes coding for the α and β subunits of the
155 photosynthetic accessory pigment C-phycocyanin (*cpcA* and *cpcB* respectively). Cool
156 temperature assemblies contained a complete copy of *cpcA*, while warm temperature assemblies
157 lacked a complete copy of the α phycocyanin subunit (Figure S6A). On the other hand, all but
158 one warm temperature isolate (LA126) had a complete copy of *cpcB,* while assemblies from cool
159 temperature isolates only had the first 25 and the last 56 amino acids from *cpcB* coded for on
160 different contigs (Figure S6B).

161 Because these differences in assembly between cool and warm temperature isolates are
162 for genes coding for accessory pigments, we compared photosystem function between
163 phenotypically distinct warm and cool temperature isolates. We measured whole-cell
164 fluorescence spectra matching C-phycocyanin across rising temperatures for cool temperature
165 strain LA31 (Topt = 27.5 °C, Tmax = 31.7 °C) and warm temperature strain LA127 (Topt = 29.7

166 °C, Tmax = 35.3 °C), using increasing fluorescence from initial levels at 22 °C as an indicator of
167 loss of photosynthetic function to heat stress. The warm temperature isolate had a lower change
168 in fluorescence at physiologically-relevant temperatures below 45 °C (Figure 3A). Fluorescence
169 for both isolates increased exponentially between 48-54 °C, before abruptly crashing to zero at
170 57 °C. This suggests that light-harvesting energetic losses to fluorescence increase as the
171 photosynthetic antenna complex becomes stressed by warming temperatures, before completely
172 disassociating at a critical high temperature and losing all fluorescence. The warm temperature
173 isolate had lower fluorescence at the fluorescence peak 54 °C (t-test, $p = 0.07$), suggesting it is
174 better able to maintain its functionality under extreme thermal stress (Figure 3A). Furthermore,
175 both isolates had differing photophysiologies when comparing the photosynthetic efficiency
176 parameter Fv/Fm (Figure 3B). When acclimated to 28° C the warm temperature isolate had
177 significantly higher values (t-test, $p = 1.04 \times 10^{-7}$), suggesting its photosystem II had a greater
178 photochemical efficiency than the cool temperature isolate. The values reported here are
179 analogous to Fv/Fm measurements reported for other marine *Synechococcus* spp. (25).
180 A closer look at the genes associated with C-phycocyanin was unable to discern the exact
181 genetic mechanism causing these measured differences in photosynthetic function. We compared
182 the closed warm temperature isolate genome (LA127) and the closed genome of the closely
183 related Chesapeake Bay strain CB0101, which revealed the majority of C-phycocyanin and
184 surrounding genes in the same orientation (Figure 4A). In all draft assemblies (short-read data
185 only), assembly failed at this exact locus (Figure 4B & C). Interestingly however, the pattern of
186 contig breakage is conserved for all draft assemblies of isolates from cool temperatures (breaking
187 within copies of *cpcB*, Figure 4B), while a distinct pattern of contig breaks is found in assemblies
188 of warm temperature isolates (breaking sooner in all cases, Figure 4C). These conserved contig-

189 breakage patterns within our cool and warm groups correlate with their measured differences in
190 thermal performance curves and photophysiology, suggesting whatever variation is consistently
191 leading to these assembly results may be involved in these phenotypic traits. Long-read
192 sequencing and assembly of all isolates may help further interrogate this region. For the two we
193 were able to attempt, although we spanned this difficult-to-assemble region for the warm
194 temperature isolate LA127, we were not able to for the cool temperature isolate LA31 (Figure
195 4D), preventing a direct comparison.

196 Mapping Illumina short-reads from all isolates to single complete copies of *cpcA* and
197 *cpcB* from draft assemblies showed some single nucleotide variants (SNVs; Supplemental Note 1
198 and Figure S7); however, no SNVs were detected when mapping short-reads to this locus on the
199 closed genome from LA127 (Supplemental Note 1 and Figure S8). This suggests that although
200 minor sequence differences were detected between the complete copies of these genes recovered
201 in the closed hybrid genome (Table S5 & S6), they were identical to the completely assembled
202 copies in the draft assemblies (Table S7). Mapping rates were used to attempt to detect different
203 gene copy numbers at this locus which might contribute to this systematic pattern contig
204 breakage (Supplemental Note 2); however, these data were inconclusive. Copy numbers of *cpcA*
205 and *cpcB* vary across Subcluster 5.2 genomes (Table S8) and these isolates appear to have
206 multiple copies of the genes (Figures S7-S10; Supplemental Note 2); however, we were not able
207 to deduce from these data whether or not copy number differed between isolates from different
208 temperatures. Although the exact genomic differences causing these assembly results are as yet
209 unclear, these contig breaks occur systematically between cool and warm temperature isolates.
210 As this correlates with the observed temperature responses (Figure 1), it suggests that genes

211 associated with accessory pigment C-phycocyanin production could be involved in thermal
212 adaptation.

213 **Discussion**

214 This study demonstrates the coexistence of distinct thermal phenotypes within a highly
215 genetically similar, single population of coastal cyanobacteria. The division of this estuarine
216 *Synechococcus* population into contrasting cool and warm thermotypes was revealed following
217 incubation experiments at 18 °C and 30 °C, in which strain-sorting was identified by culture
218 isolations and thermal phenotype determinations in the laboratory. By using high-coverage short
219 reads as well as long reads to reconstruct these isolates' genomes, we found that this striking
220 phenotypic divergence between thermotypes appears to be tied to very minor genetic differences.
221 Although previous work has established that distinct functionally-relevant ecotypes coexist
222 within populations of picocyanobacteria (e.g. Kashtan et al., 2014; Thompson & Kouba, 2019),
223 this is the first study to report coexisting ecotypes at this high level of genomic resolution.

224 Variation in assembly of the genomic region containing genes coding for C-phycocyanin
225 correlated with isolation temperature and measured thermal phenotype. In addition, we measured
226 distinct differences in both thermal resilience of the phycobilisome accessory pigment complex
227 and photosynthetic efficiency (Fv/Fm) between the two thermal ecotypes isolated from different
228 temperatures. These genomic and photophysiological differences are consistent with previous
229 work examining thermal adaptation in marine *Synechococcus*. For instance, it has been suggested
230 that differences in light-harvesting machinery can explain the global distribution of
231 *Synechococcus* clades across large temperature differences (27, 28), and variation in a single
232 amino acid in either the α and β units of R-phycocyanin, an ortholog of C-phycocyanin,
233 correlated with *Synechococcus* thermal adaptation (29). Pittera et al. (2017) also found that at

234 elevated temperatures a tropical, low-latitude strain had lower fluorescence of the antenna
235 pigment complex (indicating more efficient photosynthetic energy capture) than a sub-polar
236 strain. This is similar to the trend we observed between warm and cool temperature phenotypes
237 in our study (29). Further supporting the role of phycocyanin in *Synechococcus* thermal
238 adaptation, it has been observed that intracellular concentrations of phycobilisome proteins
239 increase under high temperatures (25). It should also be noted that there could be additional, non-
240 genomic factors such as epigenetic effects not tested for in this study that can increase
241 phenotypic heterogeneity within a population, even at a high degree of relatedness. For instance,
242 epigenetic differences have sometimes been found to be associated with bacterial stress
243 responses (30, 31).

244 Although our experimental setup precludes looking at the relative abundance of each
245 ecotype in the original population, we note that the one isolate collected directly from the
246 environment was the cool temperature ecotype. In an environmental context, the average
247 summertime surface water temperature at our sample site for the period from 1957 to 2019 was
248 20.6 °C, with a maximum of 26.5 °C (Figure 5A). This distribution of temperatures falls below
249 the Topt for both ecotypes, but would likely favor cool temperature isolates. Warm temperature
250 isolates were also collected from 30 °C enrichments, 3.5 °C above the highest measured
251 temperature at this site. Average summer SST at this site has been increasing at a rate of 0.03 °C
252 per year since 1957 (Figure 5A), meaning that the average summertime SST in Narragansett Bay
253 will likely increase to ~23 °C by the end of the century. Assuming a similar distribution of
254 temperatures in the year 2100, there will be periods when SST is above the average Topt of the
255 low temperature ecotype, and conditions will favor the high temperature ecotype (Figure 5B).

256 Any continued trend of rising temperatures beyond 2100 will continue to further expand the
257 niche of the warm temperature ecotype.

258 In addition to this intraspecific diversity likely increasing the resilience of this population
259 to long term warming trends, it is also interesting to consider why adaptations to temperatures
260 exceeding current thermal maxima are maintained in this population. The higher growth rates of
261 cool temperature isolates under typical summer conditions suggest that having the warm
262 temperature phenotype has a fitness cost (when defined purely by growth rates), and in theory
263 selection (considering only growth rates) should remove this phenotype from the population
264 (Innan & Kondrashov, 2010 and references therein). Given the temperature trends at this site, it
265 seems unlikely these are seasonal ecotypes, as the shape of thermal curves suggest that the warm
266 temperature phenotype only has a growth advantage above the maximum daily high temperature
267 observed (26.5 °C).

268 An intriguing explanation for this thermal diversity is that these microbes originated in
269 warmer low latitude waters, and were advected into this relatively cooler region as part of the
270 northerly flow of the nearby Gulf Stream. It has been estimated that microbes entrained in the
271 Gulf Stream may experience a range of temperatures as a result of advection that is larger than
272 changes due to seasonal patterns (33). Although Narragansett Bay is a narrow coastal estuary,
273 wind-driven circulation during summer months facilitates persistent exchange between estuarine
274 waters in the Bay and oceanic waters in Rhode Island Sound (34). This has led to the conjecture
275 that allochthonous inputs of sub-tropical phytoplankton could occur (35, 36), which is supported
276 by the well documented recurring appearance of subtropical fish species in Narragansett Bay
277 during the summer (37).

278 These coexisting temperature phenotypes are also interesting in the context of marine
279 *Synechococcus* evolution, as temperature is thought to be a key driver of diversity between
280 clades within this group (8, 27). It is possible that intraspecific microdiversity of thermal
281 phenotypes could have been a contributing mechanism in the diversification of *Synechococcus*
282 into the distinct lineages observed today. When a population consisting of multiple thermotypes
283 encounters a novel thermal environment, one phenotype may be selected over another,
284 potentially leading to genetic divergence and speciation. Further studies will be needed on
285 intraspecific microdiversity at this level, between nearly identical strains, to assess its potential
286 role in the evolution of *Synechococcus* and marine microbes in general.
287 Our findings also have implications for our general understanding of biological responses
288 to rising temperatures. It has been shown that there can be a greater diversity of responses to
289 ocean acidification between ecotypes within phytoplankton taxonomic and functional groups,
290 than between them (Schaum et al. 2013, Hutchins et al. 2013). Our findings show that ecotypes
291 with distinct responses to climate warming can co-occur within a single population. This
292 microdiversity in thermal traits also has been detected in other marine phytoplankton. In a
293 similar study conducted within Narragansett Bay, thermal performance curves of recently
294 isolated strains of the diatom genus *Skeletonema* were compared and showed a similar high
295 degree of intraspecific diversity of thermal traits (39). This study also observed a similar
296 significant difference in thermal maxima (Tmax) across strains, and suggested that variability at
297 such thermal limits plays an important role in both ecological and biogeochemical dynamics.
298 Because of the high degree of genetic similarity between these isolates, amplicon sequencing or
299 metagenomic microbial surveys would not be able to detect this level of functional
300 microdiversity.

301 Taking together, the findings of the current study and those of the aforementioned diatom
302 study (39) suggests that this type of fine-scale variation may be widespread among marine
303 microbial taxa. In the case of our estuarine *Synechococcus*, this cryptic thermal microdiversity
304 will likely contribute to this population's ability to continue occupying its picoplanktonic niche
305 even in the face of considerable increases in environmental temperatures. Another important
306 implication is that culture studies using a single isolate or strain from a population may
307 underestimate that population's resilience to warming. A better understanding of the existing
308 functional thermal diversity within populations is needed to correctly model the impact that
309 future elevated temperatures will have on microbial communities, and on the biogeochemical
310 cycles that they regulate.

311 **Methods**

312 *Sampling and Cell Isolation*

313 Surface water at a temperature of 22°C and salinity of 28.48 was collected from the
314 Narragansett Bay Time Series site (latitude 41.47, longitude -71.40) on July 18th, 2017 (36).
315 Collected surface water was pre-filtered using 200µm mesh to remove debris and large grazers.
316 In order to select for multiple temperature phenotypes, we split the collected seawater into 18°,
317 22° (control), 26°, and 30° C temperature treatments. Incubations were performed in triplicate 2L
318 polycarbonate bottles under a 12:12 light dark cycle at 150 µmoles photons / m^2 * sec^{-1}. Cultures
319 were amended with nutrients to match F/40 media (40), and diluted semi-continuously with 0.2
320 um-filtered seawater medium when chlorophyll a fluorescence reached a predetermined
321 threshold to prevent nutrient depletion and avoid cells entering stationary phase.

322 At the time of seawater collection and after 10 days, cells from all temperature treatments
323 that were <1.5 µm in diameter with measurable phycocyanin fluorescence were sorted into 96-

324 well plates containing F/20 media (40) using a BD Influx (San Jose, CA, USA). Wells showing
325 growth over time were transferred into artificial seawater (Sunda, Price, & Morel, 2005), and
326 nutrient concentrations were gradually adjusted to F/2 levels (40). All isolates were maintained at
327 22° C at a light intensity of 150 µmoles photons / m^2 * sec^{-1}, with weekly transfers into fresh
328 culture medium.

329 *Thermal Performance Assays*

330 Thermal performance curves were obtained from 11 strains sorted from the initial surface
331 seawater and from the 18 and 30 °C treatments (Table 1). This was done by acclimating aliquots
332 of each culture for two weeks to temperatures between 9° and 33°. Temperatures >33° were
333 added where permissible. This temperature range was chosen because it exceeds that of
334 Narragansett Bay (0.5-24.6 °C, Rynearson, Flickinger, & Fontaine, 2020), and encompasses
335 projected SST increases (20). Strains were grown at each temperature in triplicate 8 ml
336 borosilicate vials containing 5ml of F/2 medium with a 12:12 light:dark cycle and 150 µmoles
337 photons / m^2 * sec^{-1}. Biomass was recorded every two days using *in vivo* chlorophyll a
338 fluorescence measured on a Turner AU-10 fluorometer (Turner Designs Inc., Sunnyvale, CA,
339 USA), and growth rates and Eppley-Norberg thermal performance curves (43) were calculated in
340 R (R Team, 2019) using the package growthTools (DOI:10.5281/zenodo.3634918). Cultures
341 containing algal contaminants (verified using fluorescence microscopy) were excluded from the
342 dataset. In two strains, LA20 and LA27, after two weeks of acclimation at 9 °C no
343 *Synechococcus* cells were observed in the culture, so the growth rate was set to zero for these
344 cultures. The thermal performance curve of each strain is hereafter referred to as its phenotype.

345 We verified growth rates for two strains, LA31 and LA127, isolated from low (18 °C)
346 and high (30 °C) temperature treatments respectively using changes in particulate organic carbon

347 (POC). Strains were grown in triplicate in 1L polycarbonate bottles for two weeks at 22 °C
348 (12:12 light:dark cycle and 150 µmoles photons / m^2 * sec^{-1}) with dilutions every three days. In
349 addition to POC, carbon fixation was also measured for both strains. Analysis for both POC and
350 carbon fixation were done as in Qu, Fu, & Hutchins (2018) and references therein. At the end of
351 two weeks, cultures were diluted to equal biomass and the temperature was increased to 28 °C.
352 Both isolates were sampled at the beginning, after two days, and after four days.
353 *DNA Extraction, Sequencing, and Analysis*
354 250ml of stationary phase culture for each strain was filtered onto 0.2 µm Polyethersulfone
355 (PES) membrane filters and DNA was extracted using the DNeasy PowerSoil kit (Qiagen,
356 Germantown, MD, USA). Sequencing was done on an Illumina Hiseq, paired-end with 150 base-
357 pair reads (2x150) with ~10 million reads per sample at Novogene Inc. (Beijing, China). The
358 quality of base calls was assessed using fastqc
359 (https://www.bioinformatics.babraham.ac.uk/projects/fastqc), and reads were assembled with
360 SPAdes version 3.13 (46). All programs were run with default settings, unless otherwise noted.
361 To assist in genome curation, reads were assigned taxonomy using Centrifuge version 1.0.4 (47)
362 trained on the "p_compressed+h+v" index (downloaded July 2019), and raw reads were mapped
363 to their assembled genomes using bowtie2 version 2.3.5 (48). The resulting assemblies were
364 curated to remove associated heterotrophs using Anvi'o version 5.5 (49) based on tetranucleotide
365 frequency, coverage, and read taxonomy. Gene calls for curated assemblies were generated using
366 Prodigal version 2.6.3 (50) which were then annotated using kofamScan version 1.1.0 (51) and
367 imported into Anvi'o.
368 In addition to the short-read Illumina sequencing, DNA was extracted from low-
369 temperature (18 °C) strain LA31 and high-temperature (30 °C) strain LA127 for long-read

370 sequencing using an Oxford Nanopore Minion (Oxford, UK) with the FLO-MIN106D flow cell.
371 Library prep was done using the Ligation Sequencing Kit (SQK-LSK109) and Rapid Barcoding
372 Kit (SQK-RBK004) following the Genomic DNA by Ligation protocol
373 (https://store.nanoporetech.com/us/media/wysiwyg/pdfs/SQK-
374 LSK109/Genomic_DNA_by_Ligation_SQK-LSK109_-minion.pdf). 200ml of culture grown to
375 stationary phase was concentrated using centrifugation (27,000 x g for 15 minutes) and extracted
376 with the GenElute Bacterial Genomic DNA Kit (Millipore Sigma, Burlington, MA, USA).
377 Basecalling was done using Guppy version 2.2.3 and long reads were filtered using filtLong
378 version 0.2.0 (https://github.com/rrwick/Filtlong). Filtered long reads were mapped to their
379 respective draft assemblies using Minimap2 version 2.17 (52), and the same was done for the
380 short reads using bowtie2 (48). Mapped long and short reads were then assembled together using
381 Unicycler version 0.4.8 (53) with subsequent gene calling and annotation performed as described
382 above.
383 In order to place our isolates in the context of the broader diversity of *Synechococcus,* we
384 pulled all *Synechococcus* genomes (a total of 78 as of July 2019) from NCBI's Refseq (Pruitt &
385 Maglott, 2001; Table S9) and placed them on a phylogenetic tree constructed with GToTree
386 version 1.4.11 (55) using concatenated amino acid sequences for 239 single copy core genes
387 specific to cyanobacteria (using the "Cyanobacteria.hmm" included within GToTree). In short,
388 genes were identified with HMMER3 version 3.2.1 (56), aligned with muscle version 3.8.1551
389 (57), trimmed with trimal 1.4 (58), and concatenated before calculating phylogenetic distance
390 using FastTree2 version 2.1.10 (59). All trees were visualized using the interactive Tree of Life
391 webpage (60). Average nucleotide identity (ANI) was calculated using fastANI version 1.2 (61).
392 The Anvi'o pangenomic pipeline (62) was used to identify gene clusters and to test for gene-

393 cluster correlations with the original incubation temperature from which each strain was isolated.
394 In addition, we looked for sequence variants at loci of interest by mapping reads to the nearest
395 phylogenetic neighbor with a complete genome and profiling single-codon-variants (SCV),
396 utilizing the framework available within Anvi'o (demonstrated at
397 http://merenlab.org/2015/07/20/analyzing-variability/).

398 *Photophysiology Measurements*

399 To analyze differences in photosynthetic accessory pigment function, 200ml of triplicate
400 cultures of low-temperature (18 °C) strain LA31 and high-temperature (30 °C) strain LA127
401 grown to stationary phase at 22 °C were concentrated by centrifuging for 15 minutes at 27,000 x
402 g. Cell pellets were then resuspended in 5ml of sterile media, and the fluorescence and
403 absorption spectra measured on a SpectraMax m2^{e} (Molecular Devices, San Jose, CA, USA). In
404 order to detect changes in efficiency in the light gathering mechanisms with temperature,
405 fluorescence was measured every three degrees from 22°-57° (10 minute incubation at each
406 temperature) following the methods of Pittera, Partensky, & Six, (2017). This large range of
407 temperatures was used in order to detect the instantaneous disassociation temperature of the
408 phycocyanin antenna complex. Fluorescence emission was measured from 600-700nm (530nm
409 excitation wavelength) matching the profile of the allophycocyanin/phycocyanin pigment
410 complex (63). In addition, we measured the photosynthetic efficiency of photosystem II (Fv/Fm)
411 for these two strains when acclimated to 28° C using a PHYTO-PAM with an excitation
412 wavelength set to 645 nm for C-phycocyanin and allophycocyanin (Heinz Walz, Effeltrich,
413 Germany). Fv/Fm measurements were made using triplicate cultures and three technical
414 replicates each that were dark acclimated for 20 minutes, as in McParland et al. (2019).

415 *Analysis of Long-term Temperature Trends*

In order to explore changes in summertime temperature trends at our study site, all available SST data from 1957 through 2019 collected as part of the long-term times series weekly measurements was downloaded from https://web.uri.edu/gso/research/plankton/data/. All measurements from June-August were aggregated by year and a simple linear model (using the lm command in R) used to calculate the rate temperature increase. The slope of this linear model was then used to predict the distribution of summertime temperature in the year 2100. A normal distribution was assumed for both present day and future temperatures, as well as a similar standard deviation from the mean.

Data and Code Availability

Curated genomes are available from SRA under the BioProject ID PRJNA566206. Isolate information and individual BioSample accession numbers can be found in Supplemental Table 2. Scripts used in the analysis and generation of all figures as well as all physiological data are available at https://figshare.com/projects/Kling_et_al_2020/66188. Phenotypic data are also available at: www.bco-dmo.org/award/712792.

Acknowledgements

This work was funded by National Science Foundation Dimensions of Biodiversity grants OCE1638804 to DAH, OCE1638834 to TR, and OCE1638958 to EL, and by OCE 1851222 to DAH and EAW. This study is based upon work conducted at the URI Marine Science Research Facility supported in part by the National Science Foundation EPSCoR awards OIA-1004057 and OIA-1655221. Illumina sequencing was supported by the Global Climate Change and Ocean Atmosphere Interaction Project, Marine Biological Sample Museum Upgrade and Expansion Project (GASI-01-02-04) to QZ and CW. Thanks to David Kehoe (Indiana University) for helpful insights into *Synechococcus* photophysiology, and to J. Cameron Thrash (University of

Southern California) and Ben Temperton (University of Exeter) for helping generate and perform base calling on Minion long reads.

References

1. J. A. Fuhrman, F. Azam, Thymidine incorporation as a measure of heterotrophic bacterioplankton production in marine surface waters: evaluation and field results. *Mar. Biol.* **66**, 109–120 (1982).
2. D. G. Capone, *et al.*, Nitrogen fixation by *Trichodesmium spp.*: An important source of new nitrogen to the tropical and subtropical North Atlantic Ocean. *Global Biogeochem. Cycles* **19** (2005).
3. K. J. Locey, J. T. Lennon, Scaling laws predict global microbial diversity. *Proc. Natl. Acad. Sci. U. S. A.* **113**, 5970–5975 (2016).
4. M. Chafee, *et al.*, Recurrent patterns of microdiversity in a temperate coastal marine environment. *ISME J.* **12**, 237–252 (2018).
5. D. M. Needham, R. Sachdeva, J. A. Fuhrman, Ecological dynamics and co-occurrence among marine phytoplankton, bacteria and myoviruses shows microdiversity matters. *ISME J.* **11**, 1614–1629 (2017).
6. T. O. Delmont, *et al.*, Single-amino acid variants reveal evolutionary processes that shape the biogeography of a global SAR11 subclade. *Elife* **8**, 1–27 (2019).
7. N. Kashtan, *et al.*, Single-cell genomics reveals hundreds of coexisting subpopulations in wild *Prochlorococcus*. *Science.* **344**, 416–420 (2014).
8. J. A. Sohm, *et al.*, Co-occurring *Synechococcus* ecotypes occupy four major oceanic regimes defined by temperature, macronutrients and iron. *ISME J.* **10**, 333 (2016).
9. N. García-García, J. Tamames, A. M. Linz, C. Pedrós-Alió, F. Puente-Sánchez,

462 Microdiversity ensures the maintenance of functional microbial communities under
463 changing environmental conditions. *ISME J.* (2019) https:/doi.org/10.1038/s41396-019-
464 0487-8.
465 10. A. Shade, *et al.*, Fundamentals of microbial community resistance and resilience. *Front.*
466 *Microbiol.* **3**, 417 (2012).
467 11. M. K. Thomas, C. T. Kremer, C. A. Klausmeier, E. Litchman, A global pattern of thermal
468 adaptation in marine phytoplankton. *Science.* **338**, 1085–1088 (2012).
469 12. D. A. Hutchins, *et al.*, Climate change microbiology—problems and perspectives. *Nat.*
470 *Rev. Microbiol.* **17**, 391 (2019).
471 13. R. Cavicchioli, *et al.*, Scientists' warning to humanity: microorganisms and climate
472 change. *Nat. Rev. Microbiol.*, 1 (2019).
473 14. A. E. Zimmerman, S. D. Allison, A. C. Martiny, Phylogenetic constraints on elemental
474 stoichiometry and resource allocation in heterotrophic marine bacteria. *Environ.*
475 *Microbiol.* **16**, 1398–1410 (2014).
476 15. D. A. Hutchins, F.-X. Fu, E. A. Webb, N. Walworth, A. Tagliabue, Taxon-specific
477 response of marine nitrogen fixers to elevated carbon dioxide concentrations. *Nat. Geosci.*
478 **6**, 790 (2013).
479 16. F.-X. Fu, *et al.*, Differing responses of marine N_2 fixers to warming and consequences for
480 future diazotroph community structure. *Aquat. Microb. Ecol.* **72**, 33–46 (2014).
481 17. N. D. Olson, *et al.*, Metagenomic assembly through the lens of validation: recent advances
482 in assessing and improving the quality of genomes assembled from metagenomes. *Brief.*
483 *Bioinform.*, 1–11 (2017).
484 18. D. A. Hutchins, F. Fu, Microorganisms and ocean global change. *Nat. Microbiol.* **2**, 17058

(2017).

19. J. D. Kling, *et al.*, Transient exposure to novel high temperatures reshapes coastal phytoplankton communities. *ISME J.* (2019) https:/doi.org/10.1038/s41396-019-0525-6.

20. R. K. Pachauri, *et al.*, *Climate change 2014: synthesis report. Contribution of Working Groups I, II and III to the fifth assessment report of the Intergovernmental Panel on Climate Change* (Ipcc, 2014).

21. M. D. Lee, *et al.*, Marine *Synechococcus* isolates representing globally abundant genomic lineages demonstrate a unique evolutionary path of genome reduction without a decrease in GC content. *Environ. Microbiol.* **21**, 1677–1686 (2019).

22. P. Flombaum, *et al.*, Present and future global distributions of the marine Cyanobacteria *Prochlorococcus* and *Synechococcus*. *Proc. Natl. Acad. Sci. U. S. A.* **110**, 9824–9829 (2013).

23. L. Guidi, *et al.*, Plankton networks driving carbon export in the oligotrophic ocean. *Nature* **532**, 465–470 (2016).

24. D. Fucich, D. Marsan, A. Sosa, F. Chen, Complete Genome Sequence of Subcluster 5.2 *Synechococcus sp.* Strain CB0101, Isolated from the Chesapeake Bay. *Microbiol. Resour. Announc.* **8**, e00484-19 (2019).

25. K. R. M. Mackey, *et al.*, Effect of temperature on photosynthesis and growth in marine *Synechococcus* spp. *Plant Physiol.* **163**, 815–829 (2013).

26. A. W. Thompson, K. Kouba, Differential Activity of Coexisting *Prochlorococcus* Ecotypes. *Front. Mar. Sci.* **6** (2019).

27. J. Pittera, *et al.*, Connecting thermal physiology and latitudinal niche partitioning in marine *Synechococcus*. *ISME J.* **8**, 1221–1236 (2014).

508 28. T. Grébert, *et al.*, Light color acclimation is a key process in the global ocean distribution
509 of *Synechococcus* cyanobacteria. *Proc. Natl. Acad. Sci. U. S. A.* **115**, E2010–E2019
510 (2018).
511 29. J. Pittera, F. Partensky, C. Six, Adaptive thermostability of light-harvesting complexes in
512 marine picocyanobacteria. *ISME J.* **11**, 112–124 (2017).
513 30. L. Hu, *et al.*, Transgenerational epigenetic inheritance under environmental stress by
514 genome-wide DNA methylation profiling in cyanobacterium. *Front. Microbiol.* **9**, 1–11
515 (2018).
516 31. J. Beaulaurier, *et al.*, Single molecule-level detection and long read-based phasing of
517 epigenetic variations in bacterial methylomes. *Nat. Commun.* **6** (2015).
518 32. H. Innan, F. Kondrashov, The evolution of gene duplications: Classifying and
519 distinguishing between models. *Nat. Rev. Genet.* **11**, 97–108 (2010).
520 33. M. A. Doblin, E. Van Sebille, Drift in ocean currents impacts intergenerational microbial
521 exposure to temperature. *Proc. Natl. Acad. Sci. U. S. A.* **113**, 5700–5705 (2016).
522 34. C. Kincaid, R. A. Pockalny, L. M. Huzzey, Spatial and temporal variability in flow at the
523 mouth of Narragansett Bay. *J. Geophys. Res. C Ocean.* **108**, 11–1 (2003).
524 35. D. G. Borkman, T. J. Smayda, Gulf Stream position and winter NAO as drivers of long-
525 term variations in the bloom phenology of the diatom *Skeletonema costatum* "species-
526 complex" in Narragansett Bay, RI, USA. *J. Plankton Res.* **31**, 1407–1425 (2009).
527 36. K. L. Canesi, T. A. Rynearson, Temporal variation of *Skeletonema* community
528 composition from a long-term time series in Narragansett Bay identified using high-
529 throughput DNA sequencing. *Mar. Ecol. Prog. Ser.* **556**, 1–16 (2016).
530 37. A. J. M. Wood, J. S. Collie, J. A. Hare, A comparison between warm-water fish

assemblages of Narragansett Bay and those of Long Island Sound waters. *Fish. Bull.* **107**, 89–100 (2009).

38. E. Schaum, B. Rost, A. J. Millar, S. Collins, Variation in plastic responses of a globally distributed picoplankton species to ocean acidification. *Nat. Clim. Chang.* **3**, 298–302 (2013).

39. S. I. Anderson, T. A. Rynearson, Variability approaching the thermal limits can drive diatom community dynamics. *Limnol. Oceanogr.*, 1–13 (2020).

40. R. R. L. Guillard, "Culture of phytoplankton for feeding marine invertebrates" in *Culture of Marine Invertebrate Animals*, (Springer, 1975), pp. 29–60.

41. W. G. Sunda, N. M. Price, F. M. M. Morel, "Trace metal ion buffers and their use in culture studies" in *Algal Culturing Techniques*, (Elsevier Academic Press London, 2005), pp. 35–63.

42. T. A. Rynearson, S. A. Flickinger, D. N. Fontaine, Metabarcoding Reveals Temporal Patterns of Community Composition and Realized Thermal Niches of *Thalassiosira Spp*. (Bacillariophyceae) from the Narragansett Bay Long - Term Plankton Time Series. **9**, 1–19 (2020).

43. J. Norberg, Biodiversity and ecosystem functioning: A complex adaptive systems approach. *Limnol. Oceanogr.* **49**, 1269–1277 (2004).

44. R. C. Team, R: A language and environment for statistical computing (2019).

45. P. Qu, F. Fu, D. A. Hutchins, Responses of the large centric diatom *Coscinodiscus sp.* to interactions between warming, elevated CO_2, and nitrate availability. *Limnol. Oceanogr.* **63**, 1407–1424 (2018).

46. A. Bankevich, *et al.*, SPAdes: a new genome assembly algorithm and its applications to

554 single-cell sequencing. *J. Comput. Biol.* **19**, 455–477 (2012).
555 47. D. Kim, L. Song, F. P. Breitwieser, S. L. Salzberg, Centrifuge: rapid and sensitive
556 classification of metagenomic sequences. *Genome Res.* **26**, 1721–1729 (2016).
557 48. B. Langmead, S. L. Salzberg, Fast gapped-read alignment with Bowtie 2. *Nat. Methods* **9**,
558 357 (2012).
559 49. A. M. Eren, *et al.*, Anvi'o: an advanced analysis and visualization platform for 'omics
560 data. *PeerJ* **3**, e1319 (2015).
561 50. D. Hyatt, *et al.*, Prodigal: prokaryotic gene recognition and translation initiation site
562 identification. *BMC Bioinformatics* **11**, 119 (2010).
563 51. T. Aramaki, *et al.*, KofamKOALA: KEGG ortholog assignment based on profile HMM
564 and adaptive score threshold. *Bioinformatics* **36**, 2251–2252 (2020).
565 52. H. Li, Minimap2: pairwise alignment for nucleotide sequences. *Bioinformatics* **34**, 3094–
566 3100 (2018).
567 53. R. R. Wick, L. M. Judd, C. L. Gorrie, K. E. Holt, Unicycler: resolving bacterial genome
568 assemblies from short and long sequencing reads. *PLoS Comput. Biol.* **13**, e1005595
569 (2017).
570 54. K. D. Pruitt, D. R. Maglott, RefSeq and LocusLink: NCBI gene-centered resources.
571 *Nucleic Acids Res.* **29**, 137–140 (2001).
572 55. M. D. Lee, GToTree: a user-friendly workflow for phylogenomics. *Bioinformatics*, 1–3
573 (2019).
574 56. S. R. Eddy, Accelerated profile HMM searches. *PLoS Comput. Biol.* **7** (2011).
575 57. R. C. Edgar, MUSCLE: multiple sequence alignment with high accuracy and high
576 throughput. *Nucleic Acids Res.* **32**, 1792–1797 (2004).

577 58. S. Capella-Gutiérrez, J. M. Silla-Martínez, T. Gabaldón, trimAl: a tool for automated
578 alignment trimming in large-scale phylogenetic analyses. *Bioinformatics* **25**, 1972–1973
579 (2009).
580 59. M. N. Price, P. S. Dehal, A. P. Arkin, FastTree 2–approximately maximum-likelihood
581 trees for large alignments. *PLoS One* **5** (2010).
582 60. I. Letunic, P. Bork, Interactive Tree Of Life (iTOL): an online tool for phylogenetic tree
583 display and annotation. *Bioinformatics* **23**, 127–128 (2006).
584 61. C. Jain, L. M. Rodriguez-R, A. M. Phillippy, K. T. Konstantinidis, S. Aluru, High
585 throughput ANI analysis of 90K prokaryotic genomes reveals clear species boundaries.
586 *Nat. Commun.* **9**, 1–8 (2018).
587 62. T. O. Delmont, A. M. Eren, Linking pangenomes and metagenomes: the *Prochlorococcus*
588 metapangenome. *PeerJ* **6**, e4320 (2018).
589 63. C. Six, *et al.*, Diversity and evolution of phycobilisomes in marine *Synechococcus spp.*: A
590 comparative genomics study. *Genome Biol.* **8** (2007).
591 64. E. L. McParland, A. Wright, K. Art, M. He, N. M. Levine, Evidence for contrasting roles
592 of dimethylsulfoniopropionate production in *Emiliania huxleyi* and *Thalassiosira*
593 *oceanica*. *New Phytol.* (2019) https:/doi.org/10.1111/nph.16374.
594
595

596 **Figures and Tables**

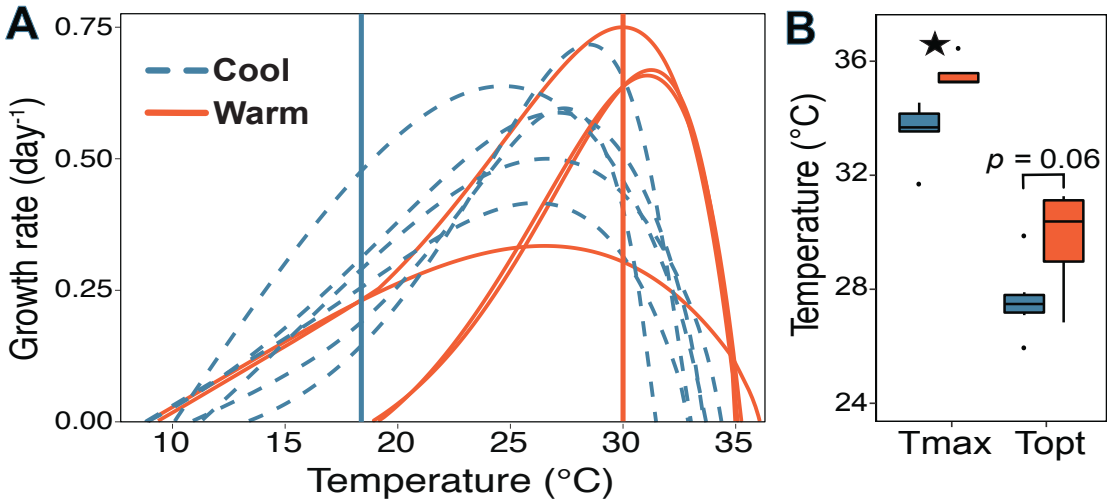

597

598 Figure 1: Thermal growth rate responses of *Synechococcus* isolates examined in this study,

599 depending on whether the isolate came from cool (blue; 18-22 °C) or warm (red; 30 °C)

600 incubation experimental temperatures. **A** Thermal Performance Curves (tpc) for all isolates

601 determined using the Eppley-Norberg approach. Vertical lines indicate 18 °C (blue) and 30 °C

602 (red). **B** Boxplots showing the maximum temperature limit (Tmax) and optimal temperature

603 (Topt) for the two sets of isolates. Error bars represent quartiles, and the star indicates $p < 0.05$

604 level (t-test).

605

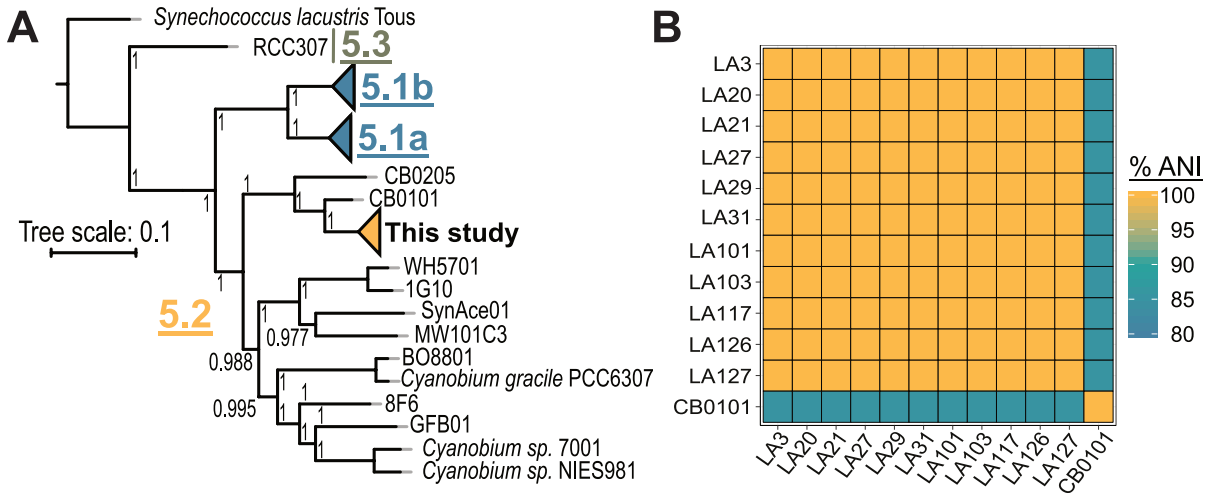

Figure 2: **A** Maximum likelihood tree showing relatedness of the three subclusters (5.1-5.3) comprising marine *Synechococcus,* using *Synechococcus lacustris* Tous to root the tree. Phylogenies were established by concatenating AA sequences of 239 single copy core genes. Scale bar shows AA change per position. **B** Average nucleotide identity (ANI) between all 11 Narragansett Bay isolates from this study. CB0101 from the Chesapeake Bay is the most closely-related genome present in Genbank and included for comparison.

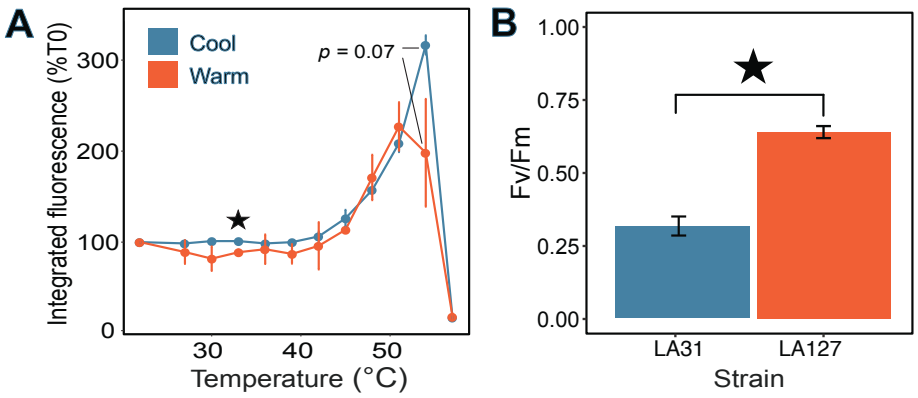

614

615 Figure 3: **A** Mean whole-cell integrated fluorescence (600-700nm) with temperature for warm

616 and cool strains and **(B)** Photochemical efficiency (Fv/Fm) of PSII at an excitation wavelength

617 matching phycocyanin and allophycocyanin (645 nm). Blue colors indicate the cool temperature

618 (18-22 °C) isolate LA31, while red shows warm temperature (30 °C) isolate LA127. The star

619 indicates observations that were statistically different (t-test, $p < 0.05$), and error bars represent ±

620 1 SD from triplicate trials.

621

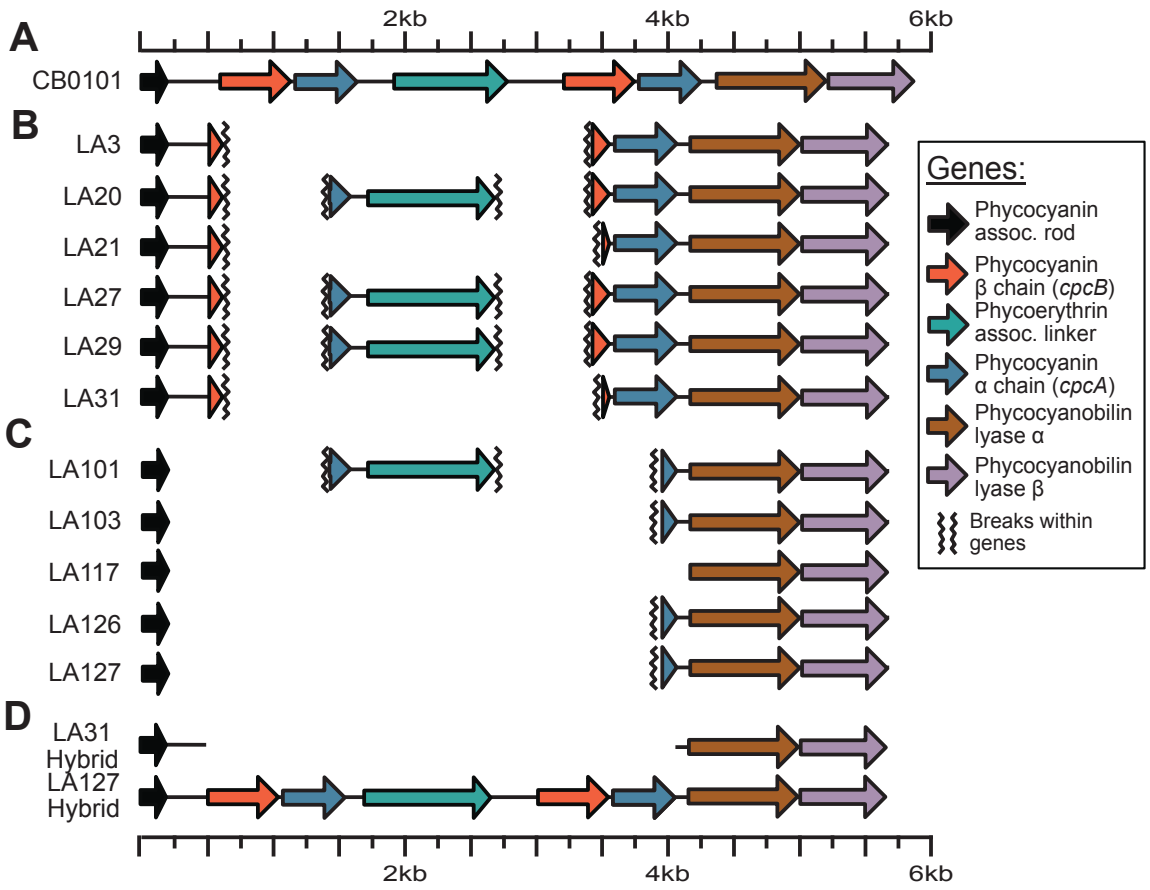

622

623 Figure 4: Assembly and coverage information of genes within the locus containing the primary

624 C-phycocyanin genes, *cpcA* (blue arrows) and *cpcB* (orange arrows). **A** C-Phycocyanin locus in

625 the closest related genome available on NCBI, CB0101. **B** Structure of draft assemblies of

626 isolates recovered from 18° or 22° **(C)** and 30° C (**D).** Same locus in a cool and warm

627 temperature strain incorporating long reads to close assembly gaps in a hybrid assembly

628 approach.

629

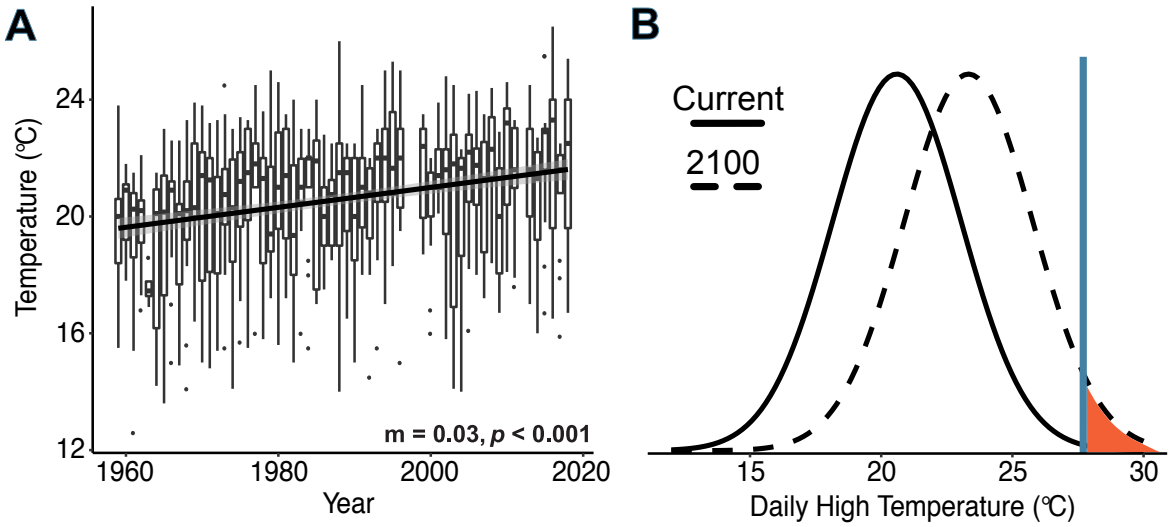

Figure 5: **A** Boxplot of summertime sea surface temperature (SST) increases at the Narragansett Bay Time Series from 1957 to 2019. Trendline shows the output of a linear model fit to the data. The slope of this model and the *p* value are shown below the data. **B** Hypothetical normal seasonal temperature distributions created using the mean of the recent data shown in panel **A** (solid line), and the predicted distribution of these data in the year 2100 (dashed line) using the slope of the linear model. A blue vertical line shows the average Topt for all cool temperature isolates. Temperatures above this line, which will likely favor warm temperature ecotypes, are shown in red.

640 Table 1: Traits derived from thermal performance curves (TPC) characterized for 11

641 *Synechococcus* isolates (indicated with n). TPC parameters are reported in °C.

Temperature	n	Parameter	Mean	SD	Max	Min
22° (Initial)	1	Tmax	33.8			
		Topt	27.9			
		Tmin	11.2			
		Width	21.8			
18°	5	Tmax	33.4	1.0	34.3	31.7
		Topt	27.6	1.4	29.8	26
		Tmin	12.4	3.1	14.8	9.0
		Width	21.0	2.5	24.5	18.9
30°	5	Tmax	35.6	0.5	36.5	35.3
		Topt	29.8	1.8	31.3	26.8
		Tmin	14.2	4.4	19.1	9.0
		Width	21.4	4.7	26.3	16.1

642